

# Design and Demonstration of a New Instrumented Spatial Linkage for Use in a Dynamic Environment: Application to Measurement of Ankle Rotations During Snowboarding

**Josh Nordquist**

Department of Mechanical Engineering,  
University of California at Davis,  
One Shields Avenue,  
Davis, CA 95616

**M. L. Hull<sup>1</sup>**

Department of Mechanical Engineering,  
and Biomedical Engineering Program,  
University of California at Davis,  
One Shields Avenue,  
Davis, CA 95616  
e-mail: mlhull@ucdavis.edu<sup>1</sup>

*Joint injuries during sporting activities might be reduced by understanding the extent of the dynamic motion of joints prone to injury during maneuvers performed in the field. Because instrumented spatial linkages (ISLs) have been widely used to measure joint motion, it would be useful to extend the functionality of an ISL to measure joint motion in a dynamic environment. The objectives of the work reported by this paper were to (i) design and construct an ISL that will measure dynamic joint motion in a field environment, (ii) calibrate the ISL and quantify its static measurement error, (iii) quantify dynamic measurement error due to external acceleration, and (iv) measure ankle joint complex rotation during snowboarding maneuvers performed on a snow slope. An "elbow-type" ISL was designed to measure ankle joint complex rotation throughout its range ( $\pm 30$  deg for flexion/extension,  $\pm 15$  deg for internal/external rotation, and  $\pm 15$  deg for inversion/eversion). The ISL was calibrated with a custom six degree-of-freedom calibration device generally useful for calibrating ISLs, and static measurement errors of the ISL also were evaluated. Root-mean-squared errors (RMSEs) were 0.59 deg for orientation (1.7% full scale) and 1.00 mm for position (1.7% full scale). A custom dynamic fixture allowed external accelerations (5 g, 0–50 Hz) to be applied to the ISL in each of three linear directions. Maximum measurement deviations due to external acceleration were 0.05 deg in orientation and 0.10 mm in position, which were negligible in comparison to the static errors. The full functionality of the ISL for measuring joint motion in a field environment was demonstrated by measuring rotations of the ankle joint complex during snowboarding maneuvers performed on a snow slope. [DOI: 10.1115/1.2486107]*

*Keywords:* instrumented spatial linkage, calibration, static, dynamic, ankle, snowboarding, error, goniometer

## Introduction

Instrumented spatial linkages (ISLs) have been widely used for measuring the total (i.e., six degrees of freedom) relative motion between body segments [1–14] (Table 1). ISLs primarily have been used to make quasi-static measurements in an environmentally controlled laboratory, a setting in which ISLs have been proven to be sufficiently accurate measurement devices.

It would be useful to extend the functionality of an ISL into measuring dynamic motion in the field environment. Joint injuries during sporting activities might be reduced by understanding the extent of the dynamic motion of joints prone to injury during maneuvers performed in the field (e.g., on a snow slope) [15–25]. An ISL might be a viable instrument for measuring dynamic joint motions if its functionality could be demonstrated in the field environment.

The field environment introduces factors that can interfere with the functionality of an ISL. Because the field environment is often dynamic, an ISL will be subjected to accelerations, which can

cause inertial loads and corresponding deflections of the ISL structural components. If large, then these deflections could introduce substantial dynamic errors into ISL measurements. Also some field environments (e.g., snow slopes) introduce extreme temperatures and moisture that can cause malfunction of electrical equipment. However, the effect of such factors can be considered in the ISL design phase and an ISL can be designed so that these factors do not interfere with its functionality. Thus, the first objective of this study was to design and construct an ISL that will measure dynamic joint motion in a field environment. Because an ISL must be designed for a specific application, an ISL was designed to measure ankle joint complex motion during snowboarding maneuvers.

To use an ISL in confidence, the device must be calibrated for its measurement environment and the measurement error quantified. If the ISL is to be used in a dynamic field environment, then the ISL must be calibrated and both static and dynamic errors must be determined. Relative motion with an ISL is calculated through matrix multiplication of a series of transformation matrices. These transformation matrices are derived from mechanical and electrical parameters of an ISL. Calibration involves measuring the relative position and orientation of known calibration configurations of an ISL and optimizing the mechanical and electrical parameter values to minimize measurement error [12,26–28].

<sup>1</sup>Corresponding author.

Contributed by the Bioengineering Division of ASME for publication in the JOURNAL OF BIOMECHANICAL ENGINEERING. Manuscript received July 14, 2005; final manuscript received June 30, 2006. Review conducted by David FitzPatrick.

**Table 1 Summary of ISLs used in previous research**

Author(s)	Year	Joint of interest	Calibration device used?	ISL error	
				Position <sup>a</sup> (mm)	Orientation (deg)
Townsend	1977	Knee	No	NA	NA
Chao	1980	hip, knee, ankle	Yes	NA	1.6
Suntay et al.	1983	knee	Yes	0.5	0.5
Kirstukas et al.	1992	knee	Yes	0.7	0.4
Siegler et al.	1996	ankle	Yes	0.5	1.2
Sholukha et al.	2004	NA	Yes	0.8	0.7

NA indicates that the information was not documented in the respective publication. <sup>a</sup>Throughout our paper, the word “position” in relation to an ISL refers to the spatial location of the origin of the moving coordinate system relative to the fixed coordinate system.

Calibration configurations are created with a calibration device, which mechanically joins with an ISL. Measurement error can then be quantified by comparing ISL position and orientation results with known calibration position and orientation quantities. The second objective was to calibrate an ISL and quantify its static measurement error.

With ISL attachment points fixed and the ISL in a known static configuration(s), dynamic error analysis involves measuring the time variation in the relative position and orientation while subjecting an ISL to a level of acceleration at frequencies expected in the measurement environment. To our knowledge, no previous study has performed a dynamic error analysis of an ISL. Therefore, it is unknown whether the errors introduced by a dynamic measurement environment are of sufficient magnitude to render an ISL unsuitable for measuring joint motions in the field. The third objective was to quantify dynamic measurement error due to external acceleration.

If static and dynamic measurement errors were deemed acceptable, then to demonstrate full functionality in the chosen field environment, the ISL should be used to measure the specified motion in this environment. Therefore, the final objective was to measure ankle joint complex rotation during snowboarding maneuvers performed on a snow slope.

**Materials and Methods**

**Design Description.** An “elbow-type” ISL was designed (Fig. 1) to measure ankle joint complex rotation throughout its range. For each of the three rotations, the ranges of motions were ±30 deg for flexion/extension, ±15 deg for internal/external rotation, and ±15 deg for inversion/eversion [11,29]. An elbow-type ISL was chosen because it is optimal in the sense that the ISL has both maximal work volume subject to a constraint on its length and well-connected workspace [30]. Well-connected workspace is defined as the ability to reach all positions and orientations in its workspace with a designated configuration. The elbow-type ISL incorporated two groupings of revolute joints—a grouping of two revolute joints at one end and a second grouping of three revolute joints at the other end. These two groupings were connected with two links attached by the sixth revolute joint (Fig. 1). Design criteria for an elbow-type ISL required that the fourth, fifth, and sixth revolute joint axes (group of three revolute joints) intersected, that the Denavit-Hartenberg twist angles,  $\alpha_m$ , were either 0 deg or 90 deg for all links, and that either the link length  $s_m$  or joint offset  $a_m$  was zero for each link [7,30].

The ISL design was further optimized so that the number of ISL revolute joints parallel to the boot rotation axis with the smallest range of motion was minimized [7]. A minimal number of revolute joints parallel to the boot rotation axis with the smallest range of motion minimizes measurement error due to transducer resolution. The internal/external rotation axis is expected to have the

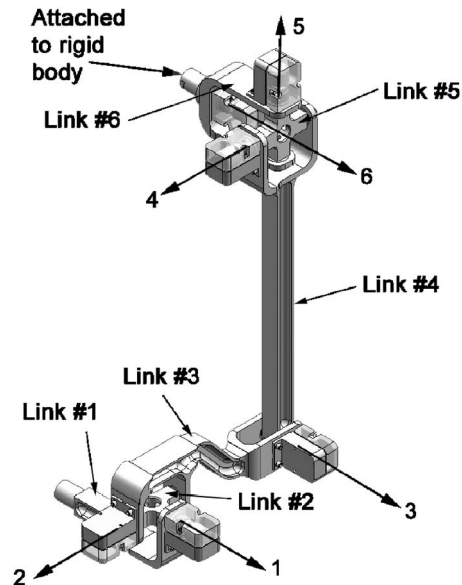


**Fig. 1** Designed elbow-type ISL, which complies with all the designated design criteria: a grouping of two revolute joints at one end (axes 1 and 2) and a grouping of three revolute joints at the other end (axes 4–6). The two groupings are connected via two links attached and the sixth revolute joint (axis 3). The fourth, fifth, and sixth revolute joint axes intersect.

smallest range of motion. The current ISL design incorporates three revolute joints parallel to the flexion/extension axis, two revolute joints parallel to the inversion/eversion axis, and one revolute joint parallel to the internal/external rotation axis.

Revolute joints in this ISL design incorporated a two-bearing compression assembly and external installation for the potentiometers chosen as the rotational transducers (model SPS12, ETI systems, Carlsbad, CA, USA). Joint compression screws were designed to compress the joint assembly (bearings and links) and provide for installation of the potentiometer (Fig. 2). Potentiometers were enclosed in protective casings, machined from Delrin (Fig. 2). These casings both protected the potentiometers from impacts and large amounts of moisture (snow) and secured the body of the potentiometer to its intended link so that it is pre-

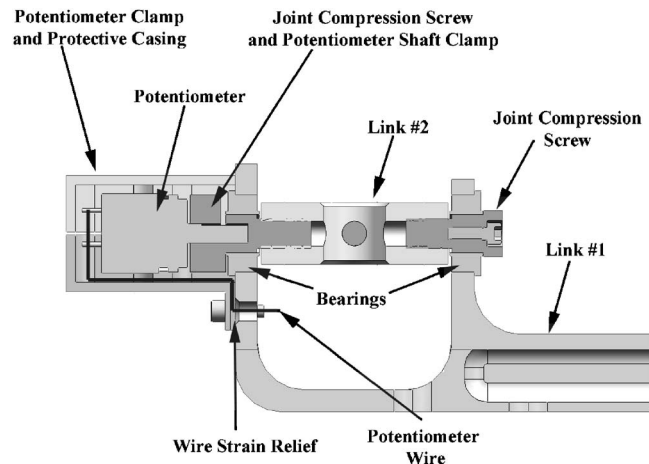


**Fig. 2** Cutaway of a revolute joint assembly illustrating the joint compression design, external potentiometer mounting, potentiometer protective casing, wire routing, and wire strain relief

vented from rotating.

Thin-wall I-beam design was used for the ISL links. The I-beam cross section offered maximal stiffness and minimal weight due to material removal in areas of the cross section that do not offer resistance to bending moments. A computer numerically controlled (CNC) milling machine (CV500, Mori Seiki, Japan) was used to manufacture these links and most of the other ISL components. CNC programs were produced via CAM software (FeatureCAM 9, EGS, Salt Lake City, UT, USA). By using 6061-T6 aluminum for the majority of components, the mass of the ISL (not including required wiring) was 0.355 kg.

Wiring of the ISL was carefully considered. To insure that wires did not restrict the motion of the ISL prior to wiring, virtual motion from a software motion module (SolidEdge V15, UGS, Plano, TX, USA) was used to provide a meaningful route for wiring to follow. The ISL was wired to minimize weight and maximize protection. Teflon-coated 18-gauge wire (similar to that found in standard Ethernet cable) was chosen to provide flexibility in movement at a minimal weight. All wires incorporated multiple points of strain-relief for safety redundancy (Fig. 2). Potentiometers were wired in parallel to prevent total data loss with a malfunctioning potentiometer.

ISL fixed and moving coordinate systems were established with the origins at each ISL fixation point (Fig. 3). Relative position and orientation between the fixed and moving coordinate systems were calculated via transformation matrices. Transformation matrices were created via the Denavit-Hartenberg system of parameters [31] and a systematic approach for developing transformation matrices of linkages [6,32]. The four Denavit-Hartenberg parameters for each link are joint offset  $a_k$ , twist angle  $\alpha_k$ , link length  $s_k$ , and revolute angle  $\theta_k$ . The transformation matrix to the  $k$  link from the  $k-1$  link is

$$[T^{k/(k-1)}] = \begin{bmatrix} 1 & 0 & 0 & 0 \\ -a_k \cos \theta_k & \cos \theta_k & \cos \alpha_k \sin \theta_k & \sin \alpha_k \sin \theta_k \\ a_k \sin \theta_k & -\sin \theta_k & \cos \alpha_k \cos \theta_k & \sin \alpha_k \cos \theta_k \\ -s_k & 0 & -\sin \alpha_k & \cos \alpha_k \end{bmatrix} \quad (1)$$

A total of seven transformation matrices are necessary to calculate the relative position and orientation between the fixed and moving coordinate systems (one for each ISL revolute joint and one for aligning fixed and moving coordinate axes at the neutral configuration) according to

$$[T^{f/m}]_{\text{ISL}} = \begin{bmatrix} 1 & 0 & 0 & 0 \\ x_r & \cos \phi_1 \cos \phi_2 - \sin \phi_1 \sin \phi_2 \sin \phi_3 & -\sin \phi_1 \cos \phi_3 & \cos \phi_1 \sin \phi_2 + \sin \phi_1 \cos \phi_2 \sin \phi_3 \\ y_r & \sin \phi_1 \cos \phi_2 + \cos \phi_1 \sin \phi_2 \sin \phi_3 & \cos \phi_1 \cos \phi_3 & \sin \phi_1 \sin \phi_2 - \cos \phi_1 \cos \phi_2 \sin \phi_3 \\ z_r & -\sin \phi_2 \cos \phi_3 & \sin \phi_3 & \cos \phi_2 \cos \phi_3 \end{bmatrix} \quad (3)$$

where  $x_r$ ,  $y_r$ , and  $z_r$  are the three relative position components (i.e., coordinates of the origin of the moving coordinate system in the fixed coordinate system) and  $\phi_1$ ,  $\phi_2$ , and  $\phi_3$  are the three relative orientation components (i.e., Cardan angles to orient the moving coordinate system coincident with the fixed coordinate system) between the fixed and moving coordinate systems.

The orientation components corresponded to anatomical rotations of the ankle joint complex. For the right leg, ankle flexion was given by angle  $\phi_1$  and was a rotation about the positive  $z_m$

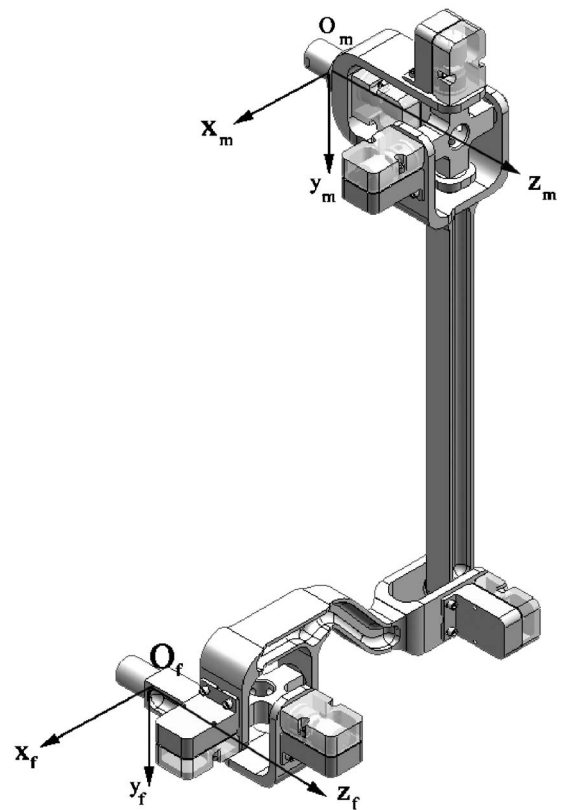


**Fig. 3** Coordinate systems that were established at both the fixed and moving ends of the ISL. Orientation of these coordinate systems was chosen to be parallel at the neutral configuration. The ISL is in the defined neutral configuration.

$$[T^{f/m}]_{\text{ISL}} = [T^{f/7}]_{\text{ISL}} [T^{7/6}]_{\text{ISL}} [T^{6/5}]_{\text{ISL}} [T^{5/4}]_{\text{ISL}} [T^{4/3}]_{\text{ISL}} \times [T^{3/2}]_{\text{ISL}} [T^{2/1}]_{\text{ISL}} [T^{1/m}]_{\text{ISL}} \quad (2)$$

The three position and three orientation components of relative motion are realized by comparison between the resulting transformation matrix and that of a general, six-parameter (three orthogonal positions, three ordered orthogonal orientations) transformation matrix given by

axis, internal rotation was given by angle  $\phi_3$  and was a rotation about the positive  $y_f$  axis, and inversion was given by angle  $\phi_2$  and was a rotation about an axis which was mutually perpendicular to the  $z_m$  and  $y_f$  axes [3]. In the neutral configuration, the relative position of the origin of the moving coordinate system in the fixed coordinate system was such that axis 2 and axis 5 (Fig. 1) were 90 deg and the origin of the moving coordinate system was in the  $x_f$ - $y_f$  plane (Fig. 3). Relative orientation between fixed and moving coordinate systems was zero in the neutral configu-

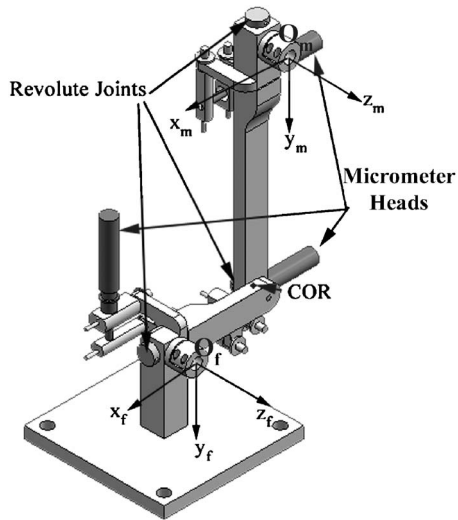


**Fig. 4 Calibration device that offers three degrees of freedom with three revolute axes that intersect at the center of rotation (COR). The calibration device is in the defined neutral position.**

ration (i.e., coordinate system axes parallel). The neutral configuration was defined as 0 deg flexion/extension, 0 deg inversion/eversion, and 0 deg internal/external rotation, as it applies to the anatomical ankle joint complex (Fig. 3).

Of the four Denavit-Hartenberg parameters for each link, the revolute joint angles  $\theta_k$  are variable and hence were measured continuously by the potentiometers. The potentiometer voltage is related to the revolute angle by

$$\theta_k = m_k V_k + b_k \quad (4)$$

where  $V_k$  is the output voltage of the transducer,  $m_k$  is the calibrated slope, and  $b_k$  is the calibrated intercept.

**Calibration and Static Error Analysis.** The design of our calibration device is a kinematic chain of three revolute joints whose axes are mutually perpendicular (Fig. 4). All three axes intersected at a point, the center of rotation, allowing simulation of a three-degree-of-freedom spherical joint. Fixation points for an ISL were offset from the center of rotation to appropriate locations to allow the center of rotation to be located at the approximate anatomical center of the ankle joint complex. Calibration device fixed and moving coordinate systems were then established that coincided with the fixed and moving coordinate systems for the ISL (Fig. 4).

The calibration device was designed and manufactured with the goal of offering sufficient precision in both position and orientation for calibrating an ISL. Components were manufactured from 6061 series aluminum with high precision, utilizing a CNC milling machine (Model CV500 accurate to 0.0013 mm, Mori Seiki, Japan) and a manual lathe with a digital readout accurate to 0.025 mm (Model Colchester 13 in., Clausing, Kalamazoo, MI, USA). Revolute joints were constructed using a double-bearing compression design, eliminating play from bearings and machining tolerances. Stainless steel, flanged, sealed, and raised inner race bearings were chosen to allow side loading of the bearing without hindering rotational motion. Revolute joint rotations were controlled via highly accurate linear micrometers (Model V63MRL, 0–50 mm, 0.002 mm resolution, Starrett, Athol, MA). Micrometer head resolution provided an overall calibration device resolution of 0.02 mm in position and 0.003 deg in orientation. Fixation for the ISL onto the calibration device was achieved using a cylindrical C-clamp design, maximizing contact area to eliminate play from machining tolerances between two mating components.

ISL calibration configurations were randomly chosen from

$\pm 30$  deg of flexion/extension rotation at 15 deg increments,  $\pm 15$  deg of internal/external rotation at 5 deg increments, and  $\pm 15$  deg of inversion/eversion rotation at 5 deg increments. The calibration device allowed for a total of 144 ISL static calibration configurations  $[(60/15=4)(30/5=6)(30/5=6)=144]$ . One hundred ISL calibration configurations were used to optimize the ISL parameters, and the remaining 44 configurations were used to quantify the measurement error of the ISL.

To optimize the accuracy of the ISL, an optimization was performed for the 38 parameters used in the overall transformation (Eq. (2)). These included five parameters for each of the six transformations involving a rotation measured by a potentiometer plus an additional four parameters for each of the other two transformations. Differences between the three position components and three orientation components established by the calibration device and those calculated via the 38 optimization parameters (termed ISL residuals) were the calibration residuals, which were included in the cost function for optimization. Calculated position components and orientation components were found by partitioning the transformation matrix (Eq. (5)) for the calibration device into two partitions, a position partition and an orientation partition, as follows:

$$[T^{f/m}]_{ISL} = \begin{Bmatrix} I & 0 \\ [P^{f/m}]_{ISL} & [R^{f/m}]_{ISL} \end{Bmatrix} \quad (5)$$

where  $[P^{f/m}]_{ISL}$  represents the position partition and  $[R^{f/m}]_{ISL}$  represents the orientation partition. In the cost function,  $J_{ISL}$ , calibration residuals (RS) were normalized to full scale range (FSR), squared, weighted ( $wt_P$  as a position weighting,  $wt_O$  as an orientation weighting), and then combined as:

$$J_{ISL} = \sum_{n=1}^e \left\{ wt_O \left[ \left( \frac{RS_{\phi_1}}{FSR_{\phi_1}} \right)^2 + \left( \frac{RS_{\phi_2}}{FSR_{\phi_2}} \right)^2 + \left( \frac{RS_{\phi_3}}{FSR_{\phi_3}} \right)^2 \right] + wt_P \left[ \left( \frac{RS_{x_r}}{FSR_{x_r}} \right)^2 + \left( \frac{RS_{y_r}}{FSR_{y_r}} \right)^2 + \left( \frac{RS_{z_r}}{FSR_{z_r}} \right)^2 \right] \right\}^2 \quad (6)$$

where  $e$  denotes the total number of calibration configurations used for parameter optimization and  $n$  denotes an individual calibration configuration. Values for weighting were chosen to be between 0 and 1, and both  $wt_O$  and  $wt_P$  were subject to the constraint given by:

$$wt_O + wt_P = 1 \quad (7)$$

Optimization was performed using a nonlinear least-squares algorithm. The algorithm was a subspace trust region method, which is based on the interior-reflective Newton method [33,34]. Calculations were performed with computational software (MATLAB 6, The Mathworks, Natick, MA, USA) and custom programs for calculations unique to the ISL. Convergence criteria of the optimization algorithm were the maximum number of iterations ( $1 \times 10^6$ ), minimum change in the cost function ( $1 \times e^{-12}$ ), or minimum value of the cost function ( $1 \times e^{-12}$ ).

Static measurement errors were calculated in the same manner as the ISL calibration residuals, differing only in that the remaining calibration configurations (not used for parameter optimization) were utilized. RMSE values were calculated for the three position components and three orientation components creating error analysis results. These error analysis results were compared for values of  $wt_O$  between 0 and 1 at 0.1 intervals. The value of  $wt_O$  that yielded the lowest error analysis results yielded the optimized parameters.

**Dynamic Error Analysis.** A dynamic fixture was designed and constructed for the dynamic error analysis (Fig. 5). The fixture oriented the ISL in the neutral configuration, while allowing for rigid ISL installment. The fixture also allowed for linear accelerations to be applied in the three acceleration directions through the

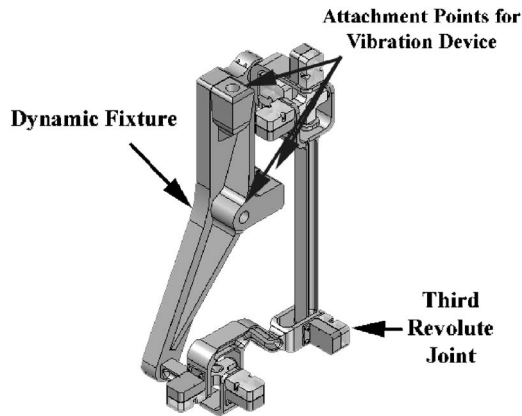


**Fig. 5** Fixture designed to provide rigid installment of the ISL and mounting points for applying external acceleration in three acceleration directions

center of mass of the ISL and dynamic fixture. Stiffness and weight of the fixture were taken into consideration, so that the fixture would not deform under the applied accelerations and the weight of both the ISL and dynamic fixture would not hinder a shaker from creating desired accelerations.

With the ISL in the neutral configuration, the natural frequencies of the ISL were measured in three directions (parallel to ISL fixed coordinate system axes) using an impact hammer test. Fixed and moving ends of the ISL were held rigidly with the dynamic fixture, while the fixture was rigidly mounted to a massive support. Impacts were applied at the third revolute joint (Fig. 5) to activate the lowest resonance of the ISL. The natural frequencies were measured using an accelerometer installed onto the ISL (installed parallel to each of the three translation directions). Output voltages from the accelerometer were collected at 1000 Hz/channel via a portable data acquisition system (DAQ700 PCMCIA, National Instruments, Austin, TX, USA, installed into a laptop).

The ISL was subjected to acceleration of 5 g over the bandwidth of 0–50 Hz in three translation directions parallel to each axis of the ISL fixed coordinate system. A meaningful magnitude and bandwidth for the dynamic calibration were determined based on previous research [35]. The 5 g magnitude was chosen to exceed the maximum acceleration of 3 g estimated from previous research. These inputs were applied with a servohydraulic actuator (model 242.1, MTS, Eden Prairie, MN, USA). Potentiometer voltages were collected at 1000 Hz/channel using the portable data acquisition system.

Collected data was filtered with a zero phase shift, low-pass Butterworth filter (order 10, cutoff frequency 55 Hz) prior to calculating relative positions and orientations. Relative position components and orientation components between the ISL fixed and moving coordinate systems were then calculated, along with the standard deviation, to determine the dynamic measurement error or deviation due to external acceleration.

**Demonstration on a Snow Slope.** The ISL was installed onto the medial side of a right step-in style snowboard boot (model: Sector, size: 44.5, K2 Sports, Vashon, WA, USA). Mounts were constructed for the ISL and installed onto the snowboard boot (ISL cuff mount and ISL sole mount). Mounting plates were incorporated into the snowboard boot sole and upper cuff to ensure a rigid mounting of the ISL mounts. Soft materials were removed from the sole of the boot and replaced with fiberglass-reinforced epoxy in order to allow a rigid mount of the ISL sole mount (Fig. 6(a)). A fiberglass-reinforced plate was molded to fit between the inner and outer liners of the boot in the upper cuff and offered a rigid mounting surface for the ISL cuff mount (Fig. 6(b)). The ISL

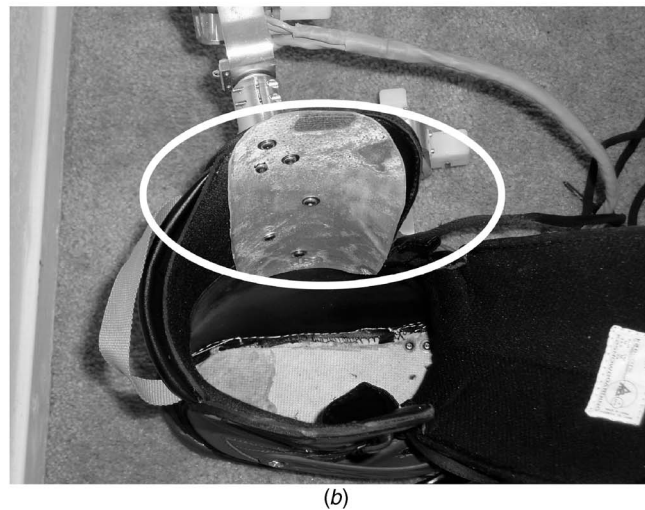
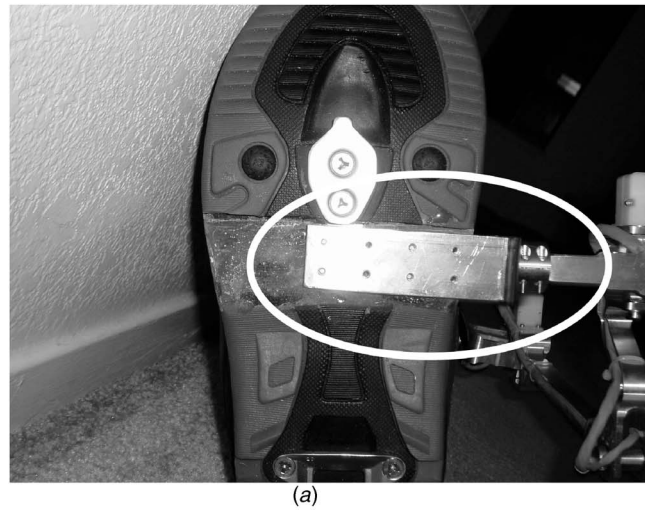


**Fig. 6 (a,b)** Modifications to the snowboard boot to accept rigid mounting of the ISL. Soft material in the sole was replaced with fiberglass-reinforced epoxy to accept the ISL sole mount (a, circled). A fiberglass-reinforced epoxy plate was molded to fit inside the boot cuff to allow a rigid mount for the ISL cuff mount (b, circled).

fixed and moving coordinate systems were installed into the ISL sole mount and cuff mount, respectively. The cuff mount was positioned so that the ISL was oriented approximately in its neutral configuration. With this mounting, flexion/extension occurred about an axis (i.e.,  $z_m$  axis) fixed to the boot cuff and perpendicular to a plane that coincided with the sagittal plane with the subject in the anatomical position, internal/external rotation occurred about an axis (i.e.,  $y_f$  axis) fixed and perpendicular to the boot sole, and inversion/eversion occurred about an axis mutually perpendicular to the other two axes.

The snow slope had an approximate angle of 30 deg, was free from moguls and clear of obstacles. Snow conditions were soft granular and packed. Weather conditions were warm (average temperature of 18°C), calm, with no appreciable wind and no precipitation.

Data from the ISL was collected for two stances: regular and goofy. Regular stance is defined as left foot forward (Fig. 7), and goofy stance is defined as right foot forward. The forward foot is the leading foot in the direction of travel on a snowboard. For each stance, the subject passed through the same course, which consisted of 12 turns (6 right and 6 left) with apexes placed ~8 m



**Fig. 7** The ISL mounted to the right snowboard boot of the subject performing a heel-side turn with a regular stance. Also visible are the ISL sole mount and cuff mount, along with the ISL data cable which travels up the right leg and into a backpack.

from the fall line and 8 m downhill from the previous apex (Fig. 8). After each run, the boot was removed from the subject until beginning the next run.

An experienced snowboarder with advanced skills was chosen as the subject. The subject was 1.85 m tall, had a mass of 74.8 kg, and was more proficient snowboarding in a regular stance than a goofy stance.

Data were acquired at 200 Hz via a portable data acquisition system (DAQCard AI 16E-4, National Instruments, Austin, TX, USA) installed into a pocket PC (model iPAQ h5550, Hewlett-Packard, Palo Alto, CA, USA) stored in a backpack. The collected data were analyzed to calculate the three snowboard boot rotations with respect to time for each of the two stances. Data were filtered with a zero phase shift, low-pass Butterworth filter (order 10, cutoff frequency 15 Hz).

## Results

**Calibration and Error Analysis.** Parameter optimization converged in 25,641 iterations. Using optimized parameters, RMSE values were 1.472 mm, 0.637 mm, and 0.906 mm for position components ( $x_r$ ,  $y_r$ , and  $z_r$  positions, respectively) (1.5%, 1.3%, and 2.3% FS, respectively) (Table 2). RMSE values for orienta-

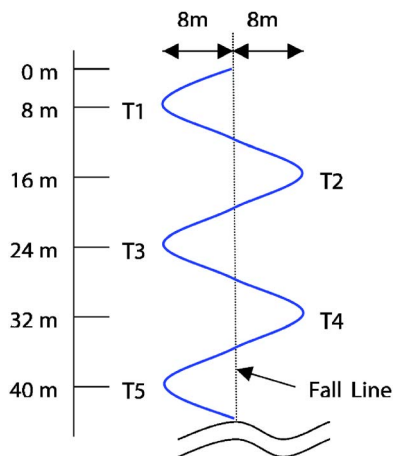


**Fig. 8** Slalom course used in measuring snowboard boot rotations in the field. The individual turns were set 8 m from the fall line and 8 m downhill from the previous turn. The slalom course had a total of 12 turns, 5 are shown here (T1-T5). For a regular stance, T1, T3, T5, etc., are heel-side turns (left foot forward). For a goofy stance, T1, T3, T5, etc., are toe-side turns (right foot forward).

**Table 2** Measures of ISL accuracy computed from the static calibration and accuracy check

Performance measure	$x_r$ (mm)	$y_r$ (mm)	$z_r$ (mm)	$\phi_1$ (deg)	$\phi_2$ (deg)	$\phi_3$ (deg)
RMSE	1.472	0.637	0.906	0.467	0.951	0.350
FSR	100.0	50.0	40.0	60.0	30.0	30.0
%FSR	1.47%	1.27%	2.27%	0.78%	3.17%	1.17%

All percents are relative to the full scale range of the respective performance measure.

tions were 0.467 deg, 0.951 deg, and 0.350 deg ( $\phi_1$ ,  $\phi_2$ , and  $\phi_3$  rotations, respectively) (0.8%, 3.2%, and 1.2% FS, respectively) (Table 2). These results were found using a  $w_{tO}$  of 0.5, which yielded the best RMSE results.

Natural frequency test results showed that the lowest natural frequency of the ISL was  $\sim 77$  Hz in the  $z_f$  direction. The natural frequencies in the  $x_f$  and  $y_f$  directions were 333 Hz and 167 Hz, respectively.

Accelerations applied in the ISL fixed  $y_f$  direction produced the largest measurement deviation. Standard deviations were 0.149 mm, 0.046 mm, and 0.095 mm for position components ( $x_r$ ,  $y_r$ , and  $z_r$  positions, respectively) and 0.070 deg, 0.039 deg, and 0.042 deg for orientations ( $\phi_1$ ,  $\phi_2$ , and  $\phi_3$  rotations, respectively) (Table 3).

**Sample Snowboard Boot Rotation Data.** The average speed of the subject snowboarding in the slalom course was 5.8 m/s. Trailing snowboard boot rotations during a regular stance maneuver show that the boot undergoes greater flexion, greater external rotation, and less inversion in combination during toe-side turns (toes are pointed toward the inside of the turn) than heel-side turns (heels are pointed toward the inside of the turn) (Fig. 9(a)). Leading snowboard boot rotations during a goofy stance maneuver show that the boot undergoes greater flexion, greater external rotation, and greater inversion in combination during toe-side turns than heel-side turns (Fig. 9(b)).

## Discussion

Although numerous ISLs have been constructed and used to measure quasi-static anatomical joint rotation, no previous study known to the authors has designed and calibrated an ISL to measure joint rotation in a dynamic environment. Therefore, the objectives of this study were to (i) design and construct an ISL that will measure dynamic joint motion in a field environment, (ii) calibrate the ISL and quantify the static measurement error, (iii) quantify dynamic measurement error due to external acceleration, and (iv) demonstrate full functionality of the ISL by measuring ankle joint complex rotations during snowboarding maneuvers performed on a snow slope. The key findings were (i) a new ISL, designed specifically for use in a dynamic environment, was manufactured using methods to insure high precision; (ii) a custom high-precision calibration device was manufactured and ISL static measurement error quantified; (iii) static calibration RMSE values are comparable to those of past ISL designs, (iv) a method for quantifying measurement error of an ISL due to external ac-

**Table 3** Measurement deviation of the ISL when subjected to external accelerations

Applied direction	$x_r$ (mm)	$y_r$ (mm)	$z_r$ (mm)	$\phi_1$ (deg)	$\phi_2$ (deg)	$\phi_3$ (deg)
$x_f$	0.149	0.046	0.095	0.070	0.039	0.042
$y_f$	0.129	0.034	0.073	0.050	0.036	0.019
$z_f$	0.112	0.030	0.082	0.048	0.041	0.018

All values are standard deviations from the mean relative positions and orientations.

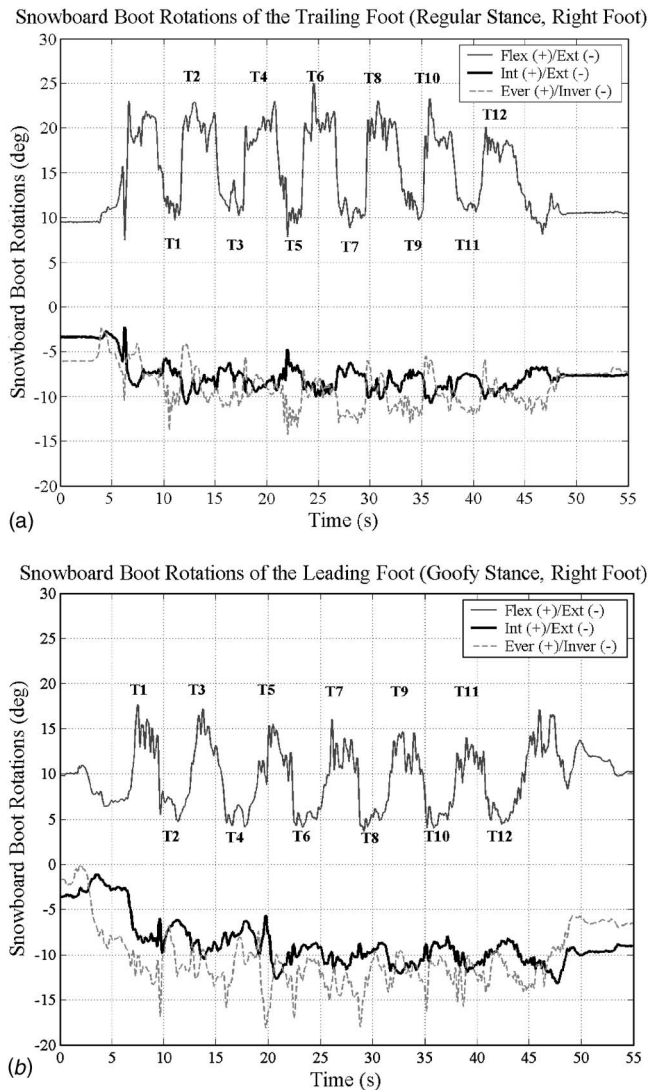


**Fig. 9 (a, b) Snowboard boot rotations of the trailing foot (a) and the leading foot (b) for a subject traveling through the slalom course (Fig. 8). The left foot is the leading foot for a regular stance, while the right foot is the leading foot for a goofy stance. These example data were collected from individual runs.**

celerations was created, (v) maximum measurement deviations were  $<0.25\%$  of full-scale range due to external accelerations, and (vi) the full functionality of the ISL in a dynamic field environment was demonstrated by successfully measuring boot rotations during snowboarding maneuvers on a snow slope. Because the functionality of the ISL is tied directly to the steps taken in design, manufacturing, and calibration to reduce measurement error in a dynamic environment, the design, manufacturing, and calibration methods will be reviewed followed by a discussion of the example data measured in the field.

**Design Requirements and Laboratory Evaluation.** Numerous efforts were taken in the design, manufacturing, and calibration of this ISL to extend its functionality into a dynamic environment. The stiffness of the ISL, which directly reduces the effect of external loading, is a combined result of revolute joint design and link design. Ideally, a revolute joint is a one-degree-of-freedom joint. However, this ideal is not achieved in practice because machining tolerances, assembly tolerances, and bearing play all contribute to an increase in the number of degrees of freedom of a

revolute joint and a subsequent increase in measurement error. Revolute joints in this ISL were compressed when assembled, which eliminated any play associated with bearing, assembly, or machining tolerances. Installing the potentiometers externally to the revolute joint eliminated potentiometer tolerances from affecting ISL measurement error and also eliminated any dependence of the stiffness of the ISL on mechanical components of the potentiometers.

The link design used in the ISL was critically assessed to offer a high stiffness-to-mass ratio so that link deformation was minimized. When subjected to inertial loads (directly proportional to mass) the links of the ISL can deform and contribute to measurement error. The longest links (specifically links 1, 3, and 4 (Fig. 1)) utilized an I-beam cross section that minimized mass while offering high bending stiffness. Individual links were monolithic, eliminating unnecessary assembly tolerances, machining tolerances, and mass.

ISL functional range of motion was determined in the design phase. A three-dimensional virtual assembly of this ISL design was created in SolidEdge V15 (UGS, Plano, TX, USA) and was imported into a motion module, which allowed motion simulations to be performed on the assembly. Harmonic motion was applied to the moving end of the ISL while the fixed end was constrained. The harmonic motion was selected so that the expected ISL workspace was fully investigated. Interferences (i.e., intersections of spatial volumes between any two components of the assembly) and clearances were calculated with the design software to insure that the design operated without interference over the full ranges of the desired motions. Motion simulations also contributed to efficient link design by allowing optimal link lengths for the specified range of motion to be determined.

Calibration methods were used to determine an optimal parameter set that can be used with confidence. Calibration was performed in the same workspace and range of motion as the ISL application. This placed the ISL in the same end-use configurations that it would experience in the application. All optimization parameters were adjusted with the use of weighting that yielded the lowest calibration residuals in the optimization procedure. These methods have been used previously to create a parameter set that does not differ greatly from the mechanically measured parameter set [26].

Static measurement errors of this ISL were similar to those published in previous studies. Studies in which multiple-degree-of-freedom calibration devices and similar calibration methods were utilized offer the most appropriate comparison. Kirstukas et al. [26] constructed a four-degree-of-freedom calibration device and presented RMSE values of 0.7 mm in position and 0.4 deg in orientation (Table 1). Kirstukas et al. calibrated the ISL within the same workspace as its end-use application. Sholukha et al. [12] constructed a multiple-degree-of-freedom calibration device and presented RSME values of 0.8 mm in position and 0.7 deg in orientation. The calibration device constructed in this work has more degrees of freedom than past devices. Nevertheless, the RMSE values are comparable (comparing Tables 1 and 2), which suggests that the calibration methods used and the measurement error results obtained are reasonable.

The method used for dynamic error analysis described in this work is new and assessed the errors of the ISL in a dynamic environment. A meaningful bandwidth for the accelerations was determined based on previous research [35]. Wang [35] used a multiple-degree-of-freedom dynamometer to collect force data between the snowboard and snowboard binding during snowboard maneuvers performed on a snow slope. The power spectrum of this data was analyzed, and the bandwidth of the force data was 0–50 Hz.

Because exciting a resonance mode of the ISL would have magnified the measurement error, the natural frequency of the ISL was measured in various modes. The lowest natural frequency was 77 Hz. Because the ISL can be modeled as a lightly damped sys-

tem, the magnification at the upper limit of the expected operating bandwidth (i.e., 50 Hz) was ~50%. Nevertheless, the ISL was sufficiently stiff that the largest measurement deviation in the dynamic calibration of 0.25% FS was an order of magnitude less than the respective static calibration RMSE. Therefore, measurement deviation in this ISL due to external accelerations applied over the bandwidth of 0–50 Hz and amplitude of 5 g is negligible.

**Example Data.** Because this study was motivated by an interest in using the ISL to better understand joint injuries, it is useful to consider the example data in this context. The most common injury to the ankle joint complex in snowboarding, which represents 12–15% of lower extremity injuries in snowboarding, is snowboarder's ankle [36,37]. The snowboarder's ankle is a fracture of the talus caused by a combination of extreme dorsiflexion and inversion of the ankle joint complex [36–40]. Though the mechanism of this injury is known, the snowboarding motion in which this injury is most common is unknown. Example snowboarding data presented here shows that dorsiflexion is most pronounced during toe-side turns of the trailing foot (Fig. 9). Furthermore, the snowboard boot offers the least resistance to motion in dorsiflexion (flexion as it applies to this study). Thus, the results of this study suggest that motions in excess of those that occur during a controlled toe-side turn could cause an injury such as snowboarder's ankle.

In this study, the ISL measured snowboard boot rotations rather than ankle joint complex rotations. Attachment of the ISL to the snowboard boot offered a noninvasive measurement technique that did not interfere with the subject's ability to perform snowboarding maneuvers. However a snowboard boot, when installed onto a subject, allows relative motions of the foot and lower shank within the boot [41,42]. Hence, to determine ankle joint complex rotations, either the ISL would have to be attached directly to the foot and shank segments or the relationship between boot rotations and corresponding ankle joint complex rotations would need to be known. This latter approach might be possible using a previously described technique for measuring relative motions between the foot and shank segments and the boot [41,42].

In summary, the contributions of this work are several. Two are that a new ISL designed to operate in a dynamic environment has been presented and a new method for quantifying the dynamic measurement error inherent to this device has been described. Results of the static and dynamic error analyses show that this ISL has comparable measurement error to past ISLs and has negligible measurement error due to external accelerations of 5 g in the bandwidth of 0–50 Hz. Thus, a third contribution of our work is demonstrating that the functionality of an ISL can be extended to a field environment. A fourth contribution is demonstrating the use of the ISL to measure snowboard boot rotations during snowboarding maneuvers on a snow slope. Because the ISL is the most commonly used goniometer for measuring multiple-degree-of-freedom motion in joints, these contributions are all important to advancing the usefulness of this goniometer in a broad spectrum of applications.

## Acknowledgment

Our gratitude goes to Matt Camalleri and Nils Hakansson in the UC Davis Biomechanical Engineering in Sports Laboratory for their technical support. Special thanks are also given to Leo Palaima and Mike Akahori of the UC Davis Student/Faculty Machine Shop for their assistance and support in manufacturing. Lastly, we acknowledge Mori Seiki Corporation of Japan for providing the CNC milling machine utilized in this project.

## References

- [1] Chao, E., 1980, "Justification of Triaxial Goniometer for the Measurement of Joint Rotation," *J. Biomech.*, **13**, pp. 989–1006.
- [2] Engebretsen, L., Lew, W. D., Lewis, J. L., and Hunter, R. E., 1989, "Knee

- Mechanics After Repair of the Anterior Cruciate Ligament. A Cadaver Study of Ligament Augmentation," *Acta Orthop. Scand.*, **60**, pp. 703–709.
- [3] Grood, E. S., and Suntay, W. J., 1983, "A Joint Coordinate System for the Clinical Description of Three-Dimensional Motions: Application to the Knee," *ASME J. Biomech. Eng.*, **105**, pp. 136–144.
- [4] Ishii, Y., Terajima, K., Koga, Y., Takahashi, H. E., Bechtold, J. E., and Gustilo, R. B., 1998, "Gait Analysis after Total Knee Arthroplasty. Comparison of Posterior Cruciate Retention and Substitution," *J. Orthop. Sci.*, **3**, pp. 310–317.
- [5] Ishii, Y., Terajima, K., Terashima, S., and Matsueda, M., 2000, "Joint Proprioception in the Elderly With and Without Hip Fracture," *J. Orthop. Trauma*, **14**, pp. 542–545.
- [6] Kinzel, G. L., Hillberry, B. M., Hall, A. S. J., Van Sickle, D. C., and Harvey, W. M., 1972, "Measurement of the Total Motion between Two Body Segments. II. Description of Application," *J. Biomech.*, **5**, pp. 283–293.
- [7] Kirstukas, S. J., Lewis, J. L., and Erdman, A. G., 1992, "6R Instrumented Spatial Linkages for Anatomical Joint Motion Measurement. Part I. Design," *ASME J. Biomech. Eng.*, **114**, pp. 92–100.
- [8] Kovalski, J. E., Gurchiek, L. R., Heitman, R. J., Hollis, J. M., and Pearsall, A. W. T., 1999, "Instrumented Measurement of Anteroposterior and Inversion-Eversion Laxity of the Normal Ankle Joint Complex," *Foot Ankle Int.*, **20**, pp. 808–814.
- [9] Lewis, J. L., Lew, W. D., and Schmidt, J., 1988, "Description and Error Evaluation of an in Vitro Knee Joint Testing System," *ASME J. Biomech. Eng.*, **110**, pp. 238–248.
- [10] Seigler, S., Lapointe, S., Nobilini, R., and Berman, A. T., 1996, "A Six-Degrees-of-Freedom Instrumented Linkage for Measuring the Flexibility Characteristics of the Ankle Joint Complex," *J. Biomech.*, **29**, pp. 943–947.
- [11] Siegler, S., Chen, J., and Schneck, C. D., 1988, "The Three-Dimensional Kinematics and Flexibility Characteristics of the Human Ankle and Subtalar Joints—Part I: Kinematics," *ASME J. Biomech. Eng.*, **110**, pp. 364–373.
- [12] Sholukha, V., Salvia, P., Hilal, I., Feipel, V., Rooze, M., and Jan, S. V., 2004, "Calibration and Validation of 6 DOFs Instrumented Spatial Linkage for Biomechanical Applications. A Practical Approach," *Med. Eng. Phys.*, **26**, pp. 251–260.
- [13] Sommer, H. J. I., and Miller, N. R., 1980, "A Technique for Kinematic Modeling of Anatomical Joints," *ASME J. Biomech. Eng.*, **102**, pp. 311–317.
- [14] Townsend, M. A., Izak, M., and Jackson, R. W., 1977, "Total Motion Knee Goniometry," *J. Biomech.*, **10**, pp. 183–193.
- [15] Estes, M., Wang, E., and Hull, M. L., 1999, "Analysis of Ankle Deflection During a Forward Fall in Snowboarding," *ASME J. Biomech. Eng.*, **121**, pp. 243–248.
- [16] Hull, M. L., 1997, "Analysis of Skiing Accidents Involving Combined Injury to the Medial Collateral and Anterior Cruciate Ligaments," *Am. J. Sports Med.*, **25**, pp. 35–40.
- [17] Kuo, C. Y., Louie, J. K., and Mote, C. D., Jr., 1983, "Field Measurements in Snow Skiing Injury Research," *J. Biomech.*, **16**, pp. 609–624.
- [18] Louie, J. K., Kuo, C. Y., Gutierrez, M. D., and Mote, C. D., Jr., 1984, "Surface Emg and Torsion Measurements During Snow Skiing: Laboratory and Field Tests," *J. Biomech.*, **17**, pp. 713–719.
- [19] Mote, C. D., Jr., and Louie, J. K., 1983, "Accelerations Induced by Body Motions During Snow Skiing," *J. Sound Vib.*, **88**, pp. 107–115.
- [20] Neptune, R. R., Wright, I. C., and van den Bogert, A. J., 2000, "The Influence of Orthotic Devices and Vastus Medialis Strength and Timing on Patellofemoral Loads During Running," *Clin. Biomech. (Los Angel. Calif.)*, **15**, pp. 611–618.
- [21] Neptune, R. R., and Kautz, S. A., 2000, "Knee Joint Loading in Forward Versus Backward Pedaling: Implications for Rehabilitation Strategies," *Clin. Biomech. (Los Angel. Calif.)*, **15**, pp. 528–535.
- [22] Maxwell, S. M., and Hull, M. L., 1989, "Measurement of Strength and Loading Variables on the Knee During Alpine Skiing," *J. Biomech.*, **22**, pp. 609–624.
- [23] Neptune, R. R., and Hull, M. L., 1992, "A New Mechanical Ski Binding With Release Sensitivity to Torsion and Bending Moments Transmitted by the Leg," *Int. J. Sport Biomech.*, **18**, pp. 331–349.
- [24] Quinn, T. P., and Mote, C. D., Jr., 1992, "Prediction of the Loading Along the Leg During Snow Skiing," *J. Biomech.*, **25**, pp. 609–611.
- [25] Wright, I. C., Neptune, R. R., Van den Bogert, A. J., and Nigg, B. M., 1998, "Passive Regulation of Impact Forces in Heel-Toe Running," *Clin. Biomech. (Los Angel. Calif.)*, **13**, pp. 521–531.
- [26] Kirstukas, S. J., Lewis, J. L., and Erdman, A. G., 1992, "6R Instrumented Spatial Linkages for Anatomical Joint Motion Measurement. 2. Calibration," *ASME J. Biomech. Eng.*, **114**, pp. 101–110.
- [27] Liu, W., and Panjabi, M. M., 1996, "On Improving the Accuracy of Instrumented Spatial Linkage System," *J. Biomech.*, **29**, pp. 1383–1385.
- [28] Sommer, H. J. I., and Miller, N. R., 1981, "A Technique for the Calibration of Instrumented Spatial Linkages Used for Biomechanical Kinematic Measurements," *J. Biomech.*, **14**, pp. 91–98.
- [29] Chen, J., Siegler, S., and Schneck, C. D., 1988, "The Three-Dimensional Kinematics and Flexibility Characteristics of the Human Ankle and Subtalar Joint—Part II: Flexibility Characteristics," *ASME J. Biomech. Eng.*, **110**, pp. 374–385.
- [30] Paden, B., and Sastry, S., 1988, "Optimal Kinematic Design of 6R Manipulators," *Int. J. Robot. Res.*, **7**, pp. 43–61.
- [31] Uicker, J. J., Denavit, J., and Hartenberg, R. S., 1964, "An Iterative Method for the Displacement Analysis of Spatial Mechanisms," *ASME J. Appl. Mech.*, **31**, pp. 309–314.

- [32] Kinzel, G. L., Hall, A. S. J., and Hillberry, B. M., 1972, "Measurement of the Total Motion Between Two Body Segments. I. Analytical Development," *J. Biomech.*, **5**, pp. 93–105.
- [33] Coleman, T. F., and Li, Y., 1994, "On the Convergence of Reflective Newton Methods for Large-Scale Nonlinear Minimization Subject to Bounds," *Math. Program.*, **67**, pp. 189–224.
- [34] Coleman, T. F., and Li, Y., 1996, "An Interior, Trust Region Approach for Nonlinear Minimization Subject to Bounds," *SIAM J. Optim.*, **6**, pp. 418–445.
- [35] Wang, E., 2002, personal communication.
- [36] Leibner, E. D., Simanovsky, N., Abu-Sneinah, K., Nyska, M., and Porat, S., 2001, "Fractures of the Lateral Process of the Talus in Children," *J. Pediatr. Orthop.*, **10**, pp. 68–72.
- [37] Weir, E., 2001, "Snowboarding Injuries: Hitting the Slopes," *Can. Med. Assoc. J.*, **164**, p. 88.
- [38] Bladin, C., Giddings, P., and Robinson, M., 1993, "Australian Snowboard Injury Database Study—A Four Year Perspective," *Am. J. Sports Med.*, **21**, pp. 701–704.
- [39] Machold, W., Kwasny, O., Gassler, P., Kolonja, A., Reddy, B., Bauer, E., and Lehr, S., 2000, "Risk of Injury Through Snowboarding," *J. Trauma*, **48**, pp. 1109–1114.
- [40] Pino, E. C., and Colville, M. R., 1989, "Snowboard Injuries," *Am. J. Sports Med.*, **17**, pp. 778–781.
- [41] Woolman, G., 2003, personal communication.
- [42] Woolman, G., Wilson, B. D., and Milburn, P., 2003, "3D Ankle Joint Motion During Controlled Snowboard Landings," *Abstract Book, 15th International Conference on Ski Trauma and Skiing Safety*, St. Moritz, International Congress Forum, St. Moritz, Abstract D1-3.